JOURNAL OF Materials CHEMISTRY

New layered vanadium oxides $M_yH_{1-y}V_3O_8{\cdot}nH_2O$ (M = Li, Na, K) obtained by oxidation of the precursor $H_2V_3O_8$†

Vanessa Legagneur, Annie Le Gal La Salle, Alain Verbaere,* Yves Piffard and Dominique Guyomard

Laboratoire de Chimie des Solides, Institut des Matériaux Jean Rouxel, Université de Nantes, B.P. 32229 - 44322 Nantes Cedex 3, France. E-mail: Alain.Verbaere@cnrs-imn.fr

Received 10th July 2000, Accepted 13th September 2000
First published as an Advance Article on the web 6th November 2000

New layered vanadium oxides were prepared at room temperature *via* either electrochemical or chemical topotactic oxidation in aqueous media of the layered, solid precursor $H_2V_3O_8$. Their formula $M_yH_{1-y}V_3O_8{\cdot}nH_2O$ (M = Li, Na, K) shows the oxidation of vanadium to occur with the removal of one hydrogen atom and with a partial exchange of the remaining proton. A structural study by powder X-ray diffraction, including a Rietveld analysis, clearly indicated that the structure of the anionic covalent layers, V_3O_8, are preserved in going from $H_2V_3O_8$ to $M_yH_{1-y}V_3O_8{\cdot}nH_2O$. In the latter compounds, all the water molecules occupy the interlayer space along with the M^+ ions.

Introduction

As part of the search for new positive electrode materials for use in rechargeable lithium batteries, a study was devoted to $H_2V_3O_8$ and several of its derivatives, and to their Li intercalation properties. $H_2V_3O_8$ was first prepared and described by Théobald and Cabala in 1970,[1] and its crystal structure was determined by the Rietveld method by Oka *et al.* in 1990.[2] $H_2V_3O_8$ was selected because vanadium oxides are excellent candidates for positive electrodes, and because the structure of $H_2V_3O_8$ (Fig. 1) consists of a stacking of V_3O_8 layers weakly bonded to each other, which could favour the mobility of species such as Li^+ between the layers. A layer is formed of chains of VO_6 distorted octahedra (chains I and II) or VO_5 distorted square pyramids (chain III) running parallel to the *b* axis and connected to each other by corner and/or edge sharing (see Fig. 1). The two protons are bonded to one oxygen atom within the V_3O_8 layer, so that the oxygen atom of a water molecule, hereafter named OW, is bonded to a vanadium atom.[2] Fig. 1 shows the OW atoms as filled circles at vertices in chain I. The layers are held together by van der Waals interactions and probably by hydrogen bonding too, indicated by dotted lines; it is very weak since the corresponding distance OW–O is 2.86 Å. As a consequence of the V–OW bond, one could expect some acidic character of the protons, and the formula is written $H_2V_3O_8$ rather than $V_3O_7{\cdot}H_2O$.

$H_2V_3O_8$ contains $1V^{IV} + 2V^{V}$, and in view of its application as an electrode material it was also of interest to modify the composition. We intended to (i) replace at least one proton by Li^+ by ion exchange, (ii) to oxidize the compound in a topotactic reaction to possibly obtain HV_3O_8, or (iii) combine oxidation and exchange to obtain for instance a new modification of LiV_3O_8. This paper presents the preparations of the new derivatives $M_yH_{1-y}V_3O_8{\cdot}nH_2O$ (M = Li, Na, K) actually obtained from the solid precursor $H_2V_3O_8$, along with their characterization. Their performances as positive electrode materials are of interest, and a detailed study of their electrochemical behavior in Li batteries will be described in a separate article.[3]

†Electronic supplementary information (ESI) available: Tables S1–S3: powder XRD patterns of oxidized compounds $M_yH_{1-y}V_3O_8{\cdot}nH_2O$ (M = Li, Na, K). See http://www.rsc.org/suppdata/jm/b0/b005559j/

Experimental

1. Synthesis of the precursor $H_2V_3O_8$

The precursor $H_2V_3O_8$ was prepared by hydrothermal treatment: $K_2S_2O_8$ and a 0.15 mol dm^{-3} aqueous solution of $VOSO_4$ were mixed in a molar ratio of 1 : 7.5 and held in a Teflon vessel enclosed in a stainless steel Berghof bomb at 200 °C for 4 days under autogeneous pressure. The green, fibrous solid formed was separated by filtration, rinsed with water, and dried in air.

2. Electrochemical oxidations of $H_2V_3O_8$

Electrochemical oxidations were performed at room temperature (RT) in a three-electrode cell which is described in detail in ref. 4. The cell is similar to a Swagelok cell and it includes a third connection for the reference electrode. A mixture of $H_2V_3O_8$, carbon black (Super P) and a binder (PVDF) were deposited onto a platinum disk (1 cm^2) serving as a current collector, with mass percentages of 85, 10, and 5 wt% for $H_2V_3O_8$, carbon black and binder, respectively. The mass *m* of $H_2V_3O_8$ deposited onto the electrode usually lies between 2 and 45 mg. For easier comparisons, the mass *m* will be expressed in mg cm^{-2} and the current density will be normalized by dividing by *m* to give values in mA cm^{-2} g^{-1}. The oxidations were made in potentiodynamic mode, controlled with a Mac-pile system (Biologic, Claix, France), at various scan rates.

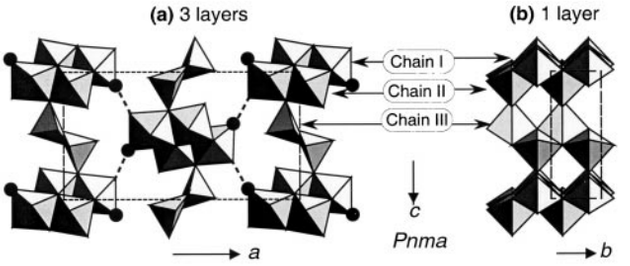

Fig. 1 Projection of the layered structure of the precursor $H_2V_3O_8$, with its VO_6 and VO_5 polyhedra: (a) [010] view showing the stacking of the layers, and the water molecule positions (filled circles) within the layers; (b) [100] view of a single layer showing the chains of polyhedra running parallel to the *b* axis. The space group is *Pnma*.

Most syntheses were realized in an aqueous solution of 0.1 mol dm^{-3} $MClO_4$ at pH close to 5.5. In order to study the influence of the cation M of the electrolyte salt on the electrochemical synthesis reaction, experiments were made with M = Li, Na, K, or TMA (tetramethylammonium), at the same concentration. Calomel (SCE), or Ag/AgCl reference electrodes were used for M = K, or M = Li, Na, TMA, respectively. For easier comparison, all measured voltages reported in this article are given with respect to the same reference SCE.

3. Chemical oxidations of $H_2V_3O_8$

The chemical oxidations were performed at RT, in aqueous media, using several oxidizing solutions providing a potential of at least 0.7 V. A suspension of 50 to 100 mg of the solid in 0.1 dm^3 of solution was stirred for approximately 1 h. In all cases a very large excess of the oxidizing agent was used. After the oxidation was complete, which was marked by a complete change from green to orange coloured solid, the product was separated by filtration, rinsed with water, and dried in air.

For the attempts at oxidation by Br_2, a solution of 0.3 cm^3 of Br_2 in 50 cm^3 H_2O was mixed with 10 mg of $H_2V_3O_8$, and the suspension was stirred for 2, 5, or 20 h.

4. Physicochemical analyses

The TG and DSC analyses were performed at a heating rate of 2 °C min^{-1}, under an air flux, using a SETARAM TG-DSC 111 system. The elemental analyses were carried out by EDX spectrometry with the use of a JEOL 5800SV scanning electron microscope. They were completed by ICP-AAS analyses, for the vanadium and alkali metal contents. The molar ratio V^V/V was determined, with a relative precision of *ca.* 2%, by redox back-titration with potentiometric detection of equivalences: the compound was first reduced with an acidic $FeSO_4$ solution and then titrated by oxidation with a $KMnO_4$ solution at pH 1.5 and 50 °C.

5. Structural study

The powder X-Ray Diffraction (XRD) patterns were recorded in reflection mode with a SIEMENS D5000 diffractometer using Cu-K_α radiation ($\lambda = 1.5406$ Å). In view of the Rietveld refinement, the pattern was recorded at RT in the 2θ range 6–120°, with steps of 0.03° (2θ) and a step time of 39 s.

The program DIFFAX[5] was used to rapidly calculate numerous theoretical powder XRD patterns resulting from various stackings of the V_3O_8 layers. The structure refinements were carried out using the program GSAS.[6] The background was fitted by fixing 20 background points. The overall parameters refined were the zero point, the cell parameters, and 7 line-profile parameters (second profile function of GSAS). As the profile of the first line at low 2θ angle could not be fitted satisfactorily, and as this strongly influenced the refinement, the 2θ range used in the refinements was limited to the domain 12–120°.

Electron diffraction patterns were obtained using a Philips CM30 microscope. The studies, which concerned samples largely dehydrated under the microscope vacuum, enabled us to obtain direct proof of the layer periodicities.

Results and discussion

1. The precursor $H_2V_3O_8$

The powder XRD pattern of the green product $H_2V_3O_8$ prepared hydrothermally is in fair agreement with that previously reported in refs. 1 and 2. The composition $H_2V_3O_8$ was confirmed by the TG analysis. The weight loss (Fig. 2) occurs in the range 220–360 °C and the resulting product at 500 °C is α-V_2O_5. The weight loss agrees with the

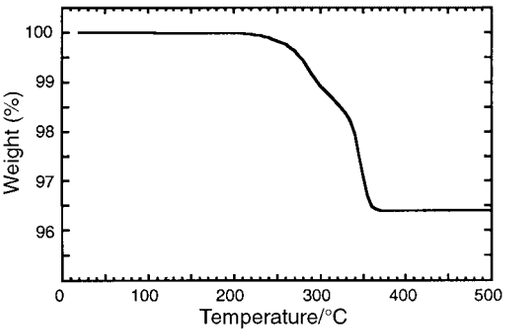

Fig. 2 Thermogravimetric analysis of the precursor $H_2V_3O_8$ (under air, heating rate of 2 °C min^{-1}).

global reaction

$$2H_2V_3O_8 + 1/2O_2 \rightarrow 3V_2O_5 + 2H_2O$$

For use as a positive electrode material in a lithium battery, it would be of interest to prepare $LiHV_3O_8$ or $Li_2V_3O_8$ from $H_2V_3O_8$, by ion exchange, since it is theoretically possible to then start the battery in charge, thus obtaining a new material HV_3O_8 or LiV_3O_8 electrochemically. Attempts were first performed by stirring a suspension of $H_2V_3O_8$ in aqueous 0.1 mol dm^{-3} LiCl solution, in the molar ratio LiCl : $H_2V_3O_8$ of 20 : 1, at 60 °C for 15 h. The resulting product showed no change in the powder XRD pattern indicating that no significant exchange occurred at 60 °C. When the reaction temperature was increased to 120 or 200 °C (the same mixture was placed in a Teflon vessel enclosed in a stainless steel Berghof bomb for 2 days), the powder XRD pattern of the product is similar to that of electrolytic V_2O_5,[7] thus showing a complete decomposition of $H_2V_3O_8$. The acidity of the protons in $H_2V_3O_8$ is not strong enough to allow the Li–H exchange under the above mentioned conditions.

2. Electrochemical oxidation of $H_2V_3O_8$

A typical first anodic scan starting from the open circuit voltage of the $H_2V_3O_8$ electrode is displayed in Fig. 3. It shows a peak near 0.65 V. This peak, which is not visible if the working electrode only contains carbon black and binder, is correlated to the oxidation of $H_2V_3O_8$. From a current (*I*) *versus* voltage (*V*) curve, the quantity of electricity, *n*(e), supplied up to a given voltage can be calculated by integration. The quantity *n*(e) will be given in electrons per $H_2V_3O_8$ formula unit. The *I*–*V* curve leads to *n*(e) = 1, in agreement with a complete V^{IV}–V^V oxidation. During the subsequent reduction scan, no current due to the reduction of the sample was observed before the reduction of water, which starts at −1 V. It can therefore be

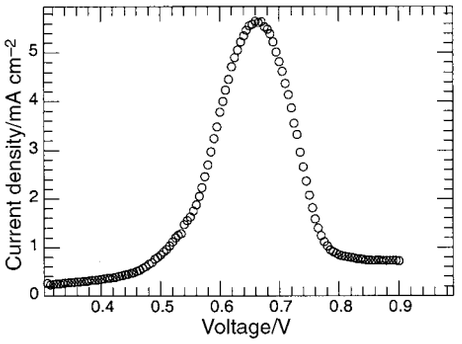

Fig. 3 Typical normalized current density *versus* voltage curve (first anodic scan) obtained at 25 °C with a composite electrode of composition ($H_2V_3O_8$: carbon black : binder) = (85 : 10 : 5 wt%), containing 45 mg cm^{-2} of $H_2V_3O_8$, scanned at 10 mV h^{-1} (pH 5.5; aqueous 0.1 mol dm^{-3} $KClO_4$).

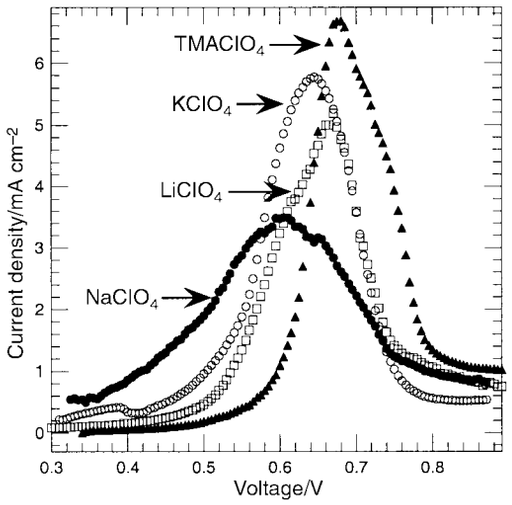

Fig. 4 Normalized current density *versus* voltage curves obtained during oxidation of the composite electrode containing $H_2V_3O_8$ in various $MClO_4$ electrolytes, M = Li, Na, K, or $(CH_3)_4N$ (TMA). (10 mV h^{-1}, 0.1 mol dm^{-3} $MClO_4$, pH 5.5, $m = 45$ mg cm^{-2}).

concluded that the electrochemical oxidation of $H_2V_3O_8$ is irreversible.

Fig. 4 shows that the position of the oxidation peak depends on the cation of the electrolyte. This result shows that the cations play a role in the oxidation mechanisms, and it strongly suggests a role in the global oxidation reaction. There is no direct, simple relationship between the peak position and the size of the cation, so the reaction most likely involves the aqueous solvation sphere of the cation. The influence of the voltage scan rate on the oxidation was also studied. Fig. 5 clearly shows that complete oxidation [n(e) = 1] does not occur at scan rates greater than *ca.* 10 mV h^{-1}.

The solid obtained in the above experiments is mixed with carbon black and binder. In view of an easier and more precise characterization, chemical oxidations were undertaken, to prepare a single phase solid.

3. Chemical oxidation of $H_2V_3O_8$

As the cation of the electrolyte plays a role in the electrochemical oxidation, several aqueous solutions were used, each of which contained M = Li, Na, or K. The first tests were performed for M = Na, with 1 mol dm^{-3} $NaClO_4$ as the oxidizing agent. The concentration of the $NaClO_4$ solution was varied from 0.1 to 1 mol dm^{-3}, which only modifies the

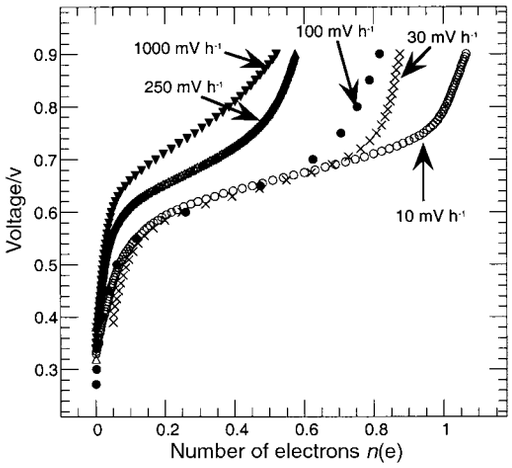

Fig. 5 Voltage *versus* n(e) curves obtained during oxidation of the composite electrode containing $H_2V_3O_8$, at various scan rates (0.1 mol dm^{-3} $KClO_4$, pH 5.5, $m = 2$ mg cm^{-2}).

Table 1 Composition and formulation, inferred from elemental analyses, redox titration, TG analyses and XRD, of all the materials prepared by oxidation of $H_2V_3O_8$

M in $MClO_{44}$	Li	Na	K
Atomic ratio M : V	0.20	0.30–(0.32)	0.20
Atomic ratio V^{IV} : V	0.00	0.00	0.00
Formula	$Li_{0.6}H_{0.4}V_3O_8{\cdot}nH_2O$	$Na_{0.9}H_{0.1}V_3O_8{\cdot}nH_2O$ ($Na_{0.96}H_{0.04}V_3O_8{\cdot}nH_2O$)	$K_{0.6}H_{0.4}V_3O_8{\cdot}nH_2O$

reaction rate: the higher the concentration, the faster the oxidation. In order to find acceptable reaction conditions, the reaction was performed at different values of pH: first the initial pH (pH 13), then $5 < pH < 6$, and also $pH < 2$. The pH was lowered by addition of concentrated HCl. The pH strongly influences the result: at the lowest pH no reaction is observed; at higher pH the oxidation occurs as revealed by a change in colour of the solid. However, as the orange coloured compound formed is soluble, the solid must be separated from the solution as soon as a single phase solid is obtained. There is a competition between the formation and dissolution of the oxidized solid, which is markedly influenced by the pH: the dissolution rate increases at increasing pH. In conclusion, an intermediate pH ($5 < pH < 6$) was used for the preparations, which ensures reasonable rates (complete oxidation within one hour and complete dissolution within two hours).

For M = Li, $LiClO_4$ was used. For similar preparations, similar results were obtained as for Na, except that the dissolution rate was much more rapid. Even at pH 5.5 and with a filtration of the solid immediately after the colour change, the yield was less than 25 wt%.

For M = K, the oxidizing agent used was 0.1 mol dm^{-3}

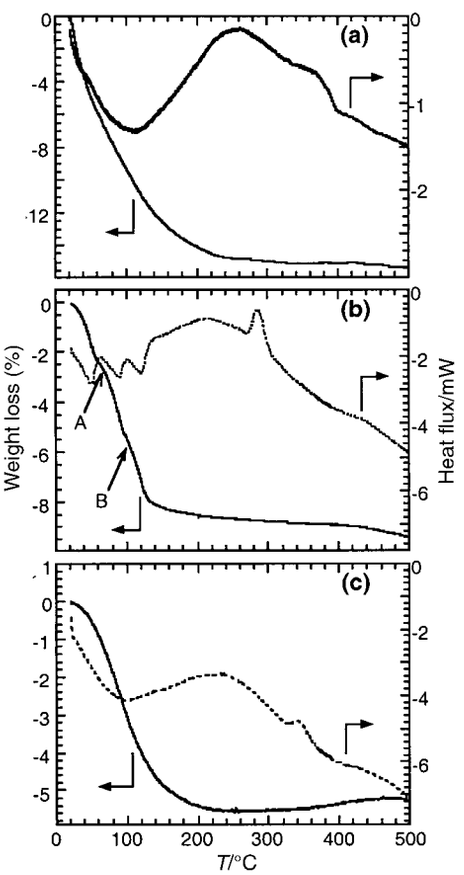

Fig. 6 TG and DSC curves (under air, at 2 °C min^{-1}) of: (a) $Li_{0.6}H_{0.4}V_3O_8{\cdot}nH_2O$, (b) $Na_{0.9}H_{0.1}V_3O_8{\cdot}nH_2O$, and (c) $K_{0.6}H_{0.4}V_3O_8{\cdot}nH_2O$.

Table 2 Unit cell parameters (orthorhombic symmetry) of the $M_yH_{1-y}V_3O_8{\cdot}nH_2O$ compounds, M = Li, Na, K

Compound	*a*/Å	*b*/Å	*c*/Å
Precursor $H_2V_3O_8$[2]	16.9298(2)	3.64432(4)	9.3589(1)
$Li_{0.6}H_{0.4}V_3O_8{\cdot}nH_2O$, $n=2.6$	21.76(1)	3.614(7)	9.36(1)
$Li_{0.6}H_{0.4}V_3O_8{\cdot}nH_2O$, $n\approx0$	18.68(9)	3.62(1)	9.38(6)
$Na_{0.9}H_{0.1}V_3O_8{\cdot}nH_2O$, $n=1.7$	22.062(3)	3.6078(6)	9.362(1)
$Na_{0.9}H_{0.1}V_3O_8{\cdot}nH_2O$, $n\approx0$	18.593(8)	3.6081(7)	9.431(4)
$K_{0.6}H_{0.4}V_3O_8{\cdot}nH_2O$, $n=1.0$	21.17(1)	3.604(1)	9.382(4)
$K_{0.6}H_{0.4}V_3O_8{\cdot}nH_2O$, $n\approx0$	19.73(3)	3.587(4)	9.267(7)

Table 3 Conditions of the last Rietveld refinement for $Na_{0.9}H_{0.1}V_3O_8{\cdot}1.7H_2O$

Unit cell parameters/Å	$a=22.058(1)$, $b=3.6078(1)$, $c=9.3619(5)$
Space group (crystal system), Z	*Pcmn* (orthorhombic) 4
R_{exp}	0.062
Refinement without structural constraint: R_{wp}/R_p	0.059/0.047
Refinement with structural parameters: $R_{wp}/R_p/R(F)/R(F^2)$	0.076/0.060/0.069/0.106
Number of independent reflections	643

$KBrO_3$. The pH of 5.5 (which is that finally retained for all the preparations, either chemical or electrochemical) was used. The reaction conditions are easier, as the oxidation rate is rapid and the dissolution rate is weak. A yield of 80 wt% is easily obtained.

As will be shown later, all the oxidation reactions above led to compounds containing the cation M of the electrolyte, or of the oxidizing reactant. In order to simply obtain HV_3O_8, without M, Br_2 was used as the oxidizing agent. The potential E_{Br^-/Br_2} is 0.82 V, however, no oxidation occured with Br_2, as the powder XRD pattern of the final product appears identical to that of $H_2V_3O_8$.

4. Physicochemical characterization of the products

Both chemical and electrochemical routes led to the same oxidized products. Furthermore, within experimental error, a unique composition was found in the products containing the same M ion (except for one Na sample, wherein the Na content is higher; the difference is small but significant, and marked by parentheses in Table 1). Results of elemental and redox analyses of the oxidized compounds are summarized in Table 1. They show that, in all cases, a large amount of cation M is incorporated in the solid phase, and the vanadium

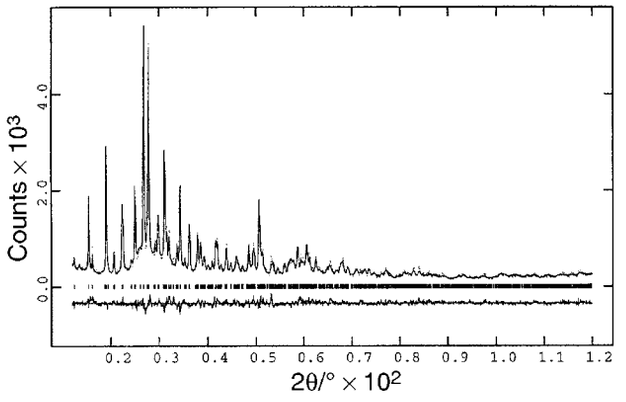

Fig. 7 Rietveld refinement plot of $Na_{0.9}H_{0.1}V_3O_8{\cdot}1.7H_2O$: observed () and calculated (—) profiles, difference on the same scale. The line positions are marked by vertical bars.

Table 4 Fractional atomic coordinates, site occupancy factors (SOF), and isotropic thermal parameters, *U*, for $Na_{0.9}H_{0.1}V_3O_8{\cdot}1.7H_2O$. OW is the oxygen atom of a water molecule

Atom	*x*	*y*	*z*	SOF	U_{iso}/Å^2
V(1)	0.0394(2)	0.25	0.1196(4)	1	0.002(1)
V(2)	0.8734(2)	0.25	0.0461(4)	1	0.013(1)
V(3)	0.4579(2)	0.75	0.0964(5)	1	0.033(2)
O(1)	0.9614(5)	0.25	0.9269(15)	1	0.011(1)
O(2)	0.0841(5)	0.25	0.276(1)	1	0.011
O(3)	0.1054(4)	0.25	0.978(1)	1	0.011
O(4)	0.9442(5)	0.25	0.213(1)	1	0.011
O(5)	0.8278(5)	0.25	0.166(1)	1	0.011
O(6)	0.8404(5)	0.25	0.889(1)	1	0.011
O(7)	0.5177(4)	0.75	0.925(1)	1	0.011
O(8)	0.3869(4)	0.75	0.037(1)	1	0.011
Na(1)	0.834(1)	0.25	0.651(3)	0.31	0.020(9)
Na(2)	0.790(1)	0.25	0.423(3)	0.35	0.005(6)
Na(3)	0.827(3)	0.75	0.713(7)	0.18	0.03(2)
Na(4)	0.811(4)	0.75	0.39(1)	0.18	0.00(2)
Na(5)	0.806(2)	0.75	0.416(7)	0.27	0.05(2)
OW(1)	0.807(2)	0.75	0.650(4)	0.42	0.05(1)
OW(2)	0.755(2)	0.75	0.363(6)	0.22	0.01(2)

is V^V only. Owing to the structural study, we must take into account a topotactic oxidation reaction, preserving the V_3O_8 layers of the precursor $H_2V_3O_8$, so that protons must ensure the charge balance in the formulas of Table 1.

The water contents, *n*, in prepared samples exposed for several days to air moisture at RT were determined by studying the thermal behaviors up to 500 °C. Fig. 6 presents the TG and DSC curves for the three different phases. For the Li and K phases they show first a large weight loss up to roughly 200 °C, due to water loss, associated with a broad, endothermic peak. For Na, this dehydration phenomenon is less simple, as it clearly occurs in three steps [Fig. 6(b)]. For the three phases, the water loss is reversible, at least up to 200 °C. The XRD pattern of the product obtained at the end of each TG analysis enables an unambiguous identification. The end product at 500 °C is:

A mixture of LiV_3O_8[8] and $Li_{0.3}V_2O_5$[9] (mainly) for $Li_{0.6}H_{0.4}V_3O_8{\cdot}nH_2O$

A mixture of NaV_3O_8[10] (mainly) and β-$Na_{0.33}V_2O_5$[11] for $Na_{0.9}H_{0.1}V_3O_8{\cdot}nH_2O$

KV_5O_{13-x}[12] for $K_{0.6}H_{0.4}V_3O_8{\cdot}nH_2O$.

The value of *n* is then inferred from the weight loss; the overall chemical formulas ar RT are: $Li_{0.6}H_{0.4}V_3O_8{\cdot}2.7H_2O$, $Na_{0.9}H_{0.1}V_3O_8{\cdot}1.7H_2O$, and $K_{0.6}H_{0.4}V_3O_8{\cdot}1.0H_2O$.

The irreversible decompositions, which occur between 200 and 500 °C are revealed by an exothermic peak on the DSC curves of Figs. 6(b) (at 285 °C) and 6(c) (at 340 °C). On Fig. 6(a), the decomposition is most likely marked by the broad peak at *ca.* 365 °C.

The Na phase has a rather good crystallinity, and several additional experiments were performed concerning its thermal behavior. On Fig. 6(b), arrows A and B show details of its TG curve, which strongly suggests the existence of particular hydrated phases. A TG curve recorded at the slower heating rate of 0.1 °C min^{-1} enabled us to observe better defined pseudo plateaus and thus to propose the compositions $Na_{0.9}H_{0.1}V_3O_8{\cdot}1.1H_2O$ and $Na_{0.9}H_{0.1}V_3O_8{\cdot}0.65H_2O$ for the phases obtained in air at 50 and 90 °C, respectively. From an XRD study of $Na_{0.9}H_{0.1}V_3O_8{\cdot}nH_2O$ at various temperatures increasing in the range 25–150 °C, it is seen that the decrease of the interlayer distance, which is associated with water loss at increasing temperature, is not observed below 50 °C. It can be concluded that a minor part of the water content at RT could be water adsorbed at the surface.

Complementary, slow heating rate experiments have shown that Li, Na, or K phases with a negligible water content can be attained at 100 °C under a primary vacuum.

Table 5 Selected interatomic distances (Å) and angles (°) in $Na_{0.9}H_{0.1}V_3O_8{\cdot}1.7H_2O$

V(1)–O(2)	1.76(1)	O(1)^{i}–V(1)–O(4)	69.0(4)		
V(1)–O(1)^{ii}	1.856(3)	O(1)^{ii}–V(1)–O(1)^{iii}	152.8(8)		
V(1)–O(1)^{iii}	1.856(3)	O(1)^{ii}–V(1)–O(2)	101.5(4)		
V(1)–O(3)	1.97(1)	O(1)^{ii}–V(1)–O(3)	81.3(4)		
V(1)–O(4)	2.27(1)	O(1)^{ii}–V(1)–O(4)	94.7(4)		
V(1)–O(1)^{i}	2.49(1)	O(1)^{iii}–V(1)–O(2)	101.5(4)		
		O(1)^{iii}–V(1)–O(3)	81.3(4)		
O(1)^{i}–V(1)–O(1)^{ii}	79.9(4)	O(1)^{iii}–V(1)–O(4)	94.7(4)		
O(1)^{i}–V(1)–O(1)^{iii}	79.9(4)	O(2)–V(1)–O(3)	98.2(6)		
O(1)^{i}–V(1)–O(2)	170.3(6)	O(2)–V(1)–O(4)	101.3(6)		
O(1)^{i}–V(1)–O(3)	91.4(5)	O(3)–V(1)–O(4)	160.4(5)		
V(2)–O(5)	1.51(1)	O(1)^{i}–V(2)–O(6)^{i}	86.4(5)		
V(2)–O(6)^{i}	1.64(1)	O(3)^{ii}–V(2)–O(3)^{iii}	147.8(6)		
V(2)–O(3)^{ii}	1.878(3)	O(3)^{ii}–V(2)–O(4)	84.9(4)		
V(2)–O(3)^{iii}	1.878(3)	O(3)^{ii}–V(2)–O(5)	104.9(4)		
V(2)–O(4)	2.21(1)	O(3)^{ii}–V(2)–O(6)^{i}	90.0(4)		
V(2)–O(1)^{i}	2.24(1)	O(3)^{iii}–V(2)–O(4)	84.9(4)		
		O(3)^{iii}–V(2)–O(5)	104.9(4)		
O(1)^{i}–V(2)–O(3)^{ii}	73.9(3)	O(3)^{iii}–V(2)–O(6)^{i}	90.0(4)		
O(1)^{i}–V(2)–O(3)^{iii}	73.9(3)	O(4)–V(2)–O(5)	86.8(5)		
O(1)^{i}–V(2)–O(4)	75.0(4)	O(4)–V(2)–O(6)^{i}	161.4(6)		
O(1)^{i}–V(2)–O(5)	161.8(6)	O(5)–V(2)–O(6)^{i}	111.8(6)		
V(3)–O(8)	1.662(9)	O(4)^{iv}–V(3)–O(7)^{v}	98.9(4)		
V(3)–O(4)^{iv}	1.81(1)	O(4)^{iv}–V(3)–O(8)	100.0(6)		
V(3)–O(7)^{ii}	1.894(4)	O(7)^{i}–V(3)–O(7)^{ii}	74.6(4)		
V(3)–O(7)^{v}	1.894(4)	O(7)^{i}–V(3)–O(7)^{v}	74.6(4)		
V(3)–O(7)^{i}	2.07(1)	O(7)^{i}–V(3)–O(8)	109.8(5)		
		O(7)^{ii}–V(3)–O(7)^{v}	144.5(7)		
O(4)^{iv}–V(3)–O(7)^{i}	150.0(5)	O(7)^{ii}–V(3)–O(8)	103.4(4)		
O(4)^{iv}–V(3)–O(7)^{ii}	98.9(4)	O(7)^{v}–V(3)–O(8)	103.4(4)		
Na(1)–O(8)^{vi}	2.11(2)	Na(2)–O(8)^{vi}	2.18(3)	Na(3)–O(2)^{ii}	1.98(8)
Na(1)–O(6)	2.23(3)	Na(2)–O(5)	2.55(2)	Na(3)–O(6)	2.46(5)
Na(1)–O(2)^{ii}	2.65(2)	Na(2)–O(6)^{ix}	2.88(3)	Na(3)–O(6)^{x}	2.46(5)
Na(1)–Na(5)	2.91(6)	Na(2)–OW(2)	2.04(3)	Na(3)–OW(2)^{xi}	2.3(1)
Na(1)–Na(5)^{viii}	2.91(6)	Na(2)–OW(2)^{viii}	2.04(3)		
				OW(1)–O(2)^{ii}	2.50(4)
Na(4)–O(8)^{vi}	2.55(6)	Na(5)–O(8)^{vi}	2.57(4)	OW(1)–O(6)	2.97(2)
Na(4)–O(8)^{vii}	2.55(6)	Na(5)–O(8)^{vii}	2.57(4)	OW(1)–O(6)^{x}	2.97(2)
Na(4)–O(5)	2.81(6)	Na(5)–O(5)	2.99(4)	OW(1)–OW(2)^{xi}	2.42(6)
Na(4)–O(5)^{x}	2.81(6)	Na(5)–O(5)^{x}	2.99(4)	OW(2)–O(6)^{ix}	2.79(2)
Na(4)–OW(1)	2.4(1)	Na(5)–OW(1)	2.18(8)	OW(2)–O(6)^{xii}	2.79(2)

Symmetry code: (i) *x*, *y*, *z*−1; (ii) 1−*x*, *1*−*y*, *1*−*z*; *(iii)* 1−*x*, −*y*, *1*−*z*; *(iv)* *x*−1/2, 1/2+*y*, *1/2*−*z*; *(v)* *1*−*x*, *2*−*y*, *1*−*z*; (vi) 1/2+*x*, *y*−1/2, 1/2−*z*; (vii) 1/2+*x*, *y*+1/2, 1/2−*z*; *(viii)* *x*, *y*−1, *z*; *(ix)* *3/2*−*x*, *y*, *z*−1/2; (x) *x*, *1*+*y*, *z*; *(xi)* *3/2*−*x*, *y*, *z*+1/2; (xii) 3/2−*x*, *y*+1, *z*−1/2.

5. Structural study

The powder XRD patterns of the oxidized compounds $M_yH_{1-y}V_3O_8{\cdot}nH_2O$ (M = Li, Na, K) are given in Tables S1–S3 (ESI). They are different from that of the precursor and they present several common features. They all show an intense line at low 2θ angle, the position of which varies reversibly with the water content (*i.e.* with the relative humidity and/or the temperature), while the position of several lines remain nearly constant. This is a typical feature of a layered hydrate in which at least a part of the H_2O is in the interlayer space. A preliminary electron diffraction study was conducted for the three phases, showing platelet shaped microcrystals; it readily indicated the in-plane periodicity is nearly the same as that in a layer of the precursor.

The XRD patterns confirm these observations; they indicate an orthorhombic symmetry, with the unit cell parameters contained in Table 2. Each as prepared phase (simply dried in air) presents the best crystallinity. The crystallinity always decreases, leading to much broader lines in the XRD pattern, when the water content has been changed by heating, even after rehydration. $Na_{0.9}H_{0.1}V_3O_8{\cdot}1.7H_2O$ is of rather good crystallinity (as compared to any other sample), and it was selected for the structural study by Rietveld refinement.

The starting structural model for the refinements was chosen in the following manner:

First, as the experimental XRD pattern is fully explained using an orthorhombic unit cell with b and c parameters close to those of $H_2V_3O_8$, we assumed that the layers in $Na_{0.9}H_{0.1}V_3O_8{\cdot}1.7H_2O$ are basically the V_3O_8 layers in $H_2V_3O_8$.

The pattern was then compared to theoretical ones calculated for various stackings of the layers, and a stacking model was retained.

Finally, the global compatibility of this model, corresponding to space group *Pcmn* (no. 62, standard setting *Pnma*), with the systematic absences of reflections in the pattern, was verified. The other possible space group $Pc2_1n$ (no. 33, standard setting $Pna2_1$), which should be used in the case of acentric distortion of the structure, was not considered.

Preliminary Rietveld refinements were performed using first the profile fitting procedure without structural information, and then introducing 3V+8O as independent positions, to obtain the stacking of V_3O_8 layers having the *Pcmn* symmetry. A subsequent difference Fourier synthesis gave information on the possible positions of the remaining atoms (Na and OW). These positions are in the interlayer space, as expected, and it is necessary to split the Na/OW positions to better account for the electron density in this region. The label Na or OW was given to the positions according the distances to their neighbouring atoms. As it is not possible to simultaneously refine the position

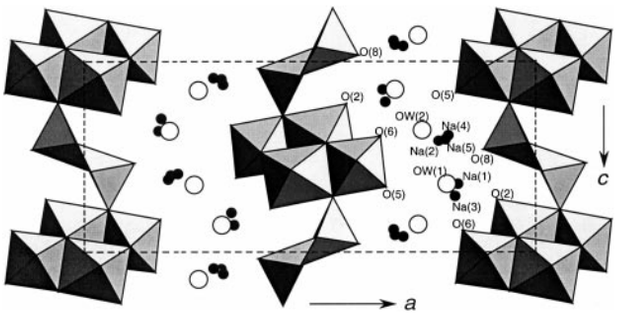

Fig. 8 [010] view of the layered structure of $Na_{0.9}H_{0.1}V_3O_8{\cdot}1.7H_2O$ showing the dominant positions of the Na^+ ions (filled circles) and of the water molecules (open circles) in the interlayer space. The space group is *Pcmn*.

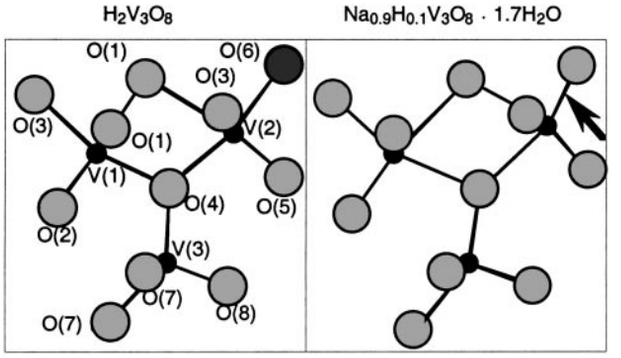

Fig. 9 Homologous structural fragments of $H_2V_3O_8$ and $Na_{0.9}H_{0.1}V_3O_8{\cdot}1.7H_2O$ showing the V–O bonding in the VO_6 and VO_5 polyhedra ([010] view).

parameters *xyz*, the isotropic thermal parameters U_{iso}, and the site occupancy factors SOF, for close Na/OW positions, systematic sets of refinement of *xyz* or U_{iso} "in turn" were performed for various, fixed SOF. Each SOF was adjusted in order to lead to plausible U_{iso} values. The refinements, without any constraint, led to 19.3 electrons in the interlayer space, while $0.9Na + 1.7H_2O$ corresponds to 23.5 electrons (assuming there is no surface water).

After the final refinement, the difference Fourier map is featureless, with maxima and minima in the range ± 1.4 e Å^{-3}. Table 3 and Fig. 7 show the Rietveld result. The global agreement between experimental and calculated profiles is satisfactory with, however, noticeable remaining peaks in the difference profile. A possible explanation for these peaks is the presence of stacking faults, which could be confirmed from the intensity of the [100] line: it is weak but not exactly zero, whereas it should be zero for space group *Pcmn*.

Tables 4 and 5 present the main structural results. Qualitatively, the structure of $Na_{0.9}H_{0.1}V_3O_8{\cdot}1.7H_2O$ still results from a stacking of the V_3O_8 layers present in $H_2V_3O_8$. Some differences concerning the two structures have to be mentioned. The space groups are different (*Pnma* and *Pcmn*), so that as compared to $H_2V_3O_8$, every second V_3O_8 layer is shifted by *b*/2 in $Na_{0.9}H_{0.1}V_3O_8{\cdot}1.7H_2O$.

The results concerning Na and OW are not precise enough (as can be seen from the standard deviations in the tables) to allow a detailed discussion of the interatomic distances. However, a comparison of the formula with the site occupancy factors obtained shows that the region of some atomic positions labeled "Na" are likely also occupied by OW. Fig. 8 illustrates the disordered situation of Na/OW between the layers, with partial occupancy of several sites.

The V–O bonding within the V_3O_8 layer is shown in Fig. 9 for both structures, with the same atom labels as in Tables 4 and 5. In this bonding scheme, oxygen atoms O(2), O(5), O(6), and O(8) are "terminal", as they are bonded to only one vanadium atom. The V–terminal O bond distance is shorter than the mean V–O distance. In ref. 2 the V(2)–O(6) distance of 2.06 Å in $H_2V_3O_8$ (Fig. 9) was judged to indicate that O(6) belongs to a water molecule. In $Na_{0.9}H_{0.1}V_3O_8{\cdot}1.7H_2O$, the corresponding distance (see the arrow on Fig. 9) is much shorter (1.64(1) Å), which gives supplementary proof of the oxidized character of $Na_{0.9}H_{0.1}V_3O_8{\cdot}1.7H_2O$. In the latter compound, H_2O is between the layers.

The other notable difference in the V–O bonding is less important, it concerns the short V(1)–O(2) distance, which is slightly shorter in $H_2V_3O_8$ [1.590(3) instead of 1.76(1) Å]. The difference seems significant and it is likely due to pertubation by close Na atoms.

A Rietveld study was also conducted for $K_{0.6}H_{0.4}V_3O_8{\cdot}1.0H_2O$. A rather satisfactory profile was calculated assuming the same structure, *i.e.* using the same space group *Pcmn* and introducing K/OW between the same V_3O_8 layers. However, all lines of the XRD pattern are broader than in the Na case, so that reliable information on the V–O bonding and on the K/OW locations could not be obtained.

The other compounds (Li phase and compounds with lower water content *n*, or anhydrous) show still broader lines, and the crystallinity precludes a precise structural study. However, their thermal behavior and the layer periodicity allow us to reasonably assume they result from a stacking of the V_3O_8 layers. The mode of stacking was not determined, likely due to stacking faults, which lower the crystal quality. This possibility was confirmed by several electron diffraction experiments, which gave evidence of diffuse streak intensity, perpendicular to the layers, in reciprocal space. Further information on the stacking in the dehydrated materials requires high resolution electron microscopy experiments.

Concluding remarks

The present study describes the synthesis of lithium intercalation materials for lithium batteries by aqueous oxidation of $H_2V_3O_8$ as a precursor. The reactions occur in the 0.6–0.7 V/SCE voltage range and are irreversible. The new oxidized hydrated solids obtained are electrochemically inactive in aqueous media. The oxidations involve the V^{IV} to V^V transformation together with the removal of one H from the solid. As the remaining proton becomes more acidic, its ion exchange with the aqueous cation M occurs. The exchange is only partial and, surprisingly, its extent is nearly constant for a given M. The solubility of $K_{0.6}H_{0.4}V_3O_8{\cdot}1.0H_2O$ being weak, a tentative ion exchange of the remaining $0.4H^+$ was performed in a KCl or KCl+KOH solution. The reaction failed.

References

1 F. Théobald and R. Cabala, *C. R. Séances Acad. Sci. Ser. C*, 1970, **270**, 2138.
2 Y. Oka, T. Yao and N. Yamamoto, *J. Solid State Chem.*, 1990, **89**, 372.
3 V. Legagneur, A. Le Gal La Salle, A. Verbaere, Y. Piffard and D. Guyomard, *J. Electrochem. Soc.*, to be published.
4 V. Legagneur, A. Le Gal La Salle, A. Verbaere, Y. Piffard and D. Guyomard, *J. Electrochem. Soc.*, accepted.
5 M. M. Treacy, J. M. Newsam and M. W. Deem, *Proc. R. Soc. London, Ser. A*, 1991, **433**, 499.
6 A. C. Larson and R. B. von Dreele, *Generalized Structure Analysis System*, University of California, Los Alamos, 1994.
7 E. Potiron, Thesis, University of Nantes, 1998.
8 A. D. Wadsley, *Acta Crystallogr.*, 1957, **10**, 261.
9 J. Galy and A. Hardy, *Bull. Soc. Chim. Fr.*, 1964, 2808.
10 G. A. Kolta, I. F. Hewaidy, N. S. Felix and N. N. Girgis, *Thermochim. Acta*, 1973, **6**, 165.
11 A. D. Wadsley, *Acta Crystallogr.*, 1955, **8**, 695.
12 V. Volkov and A. Ivakin, *Russ. J. Inorg. Chem. (Transl. of Zh. Neorg. Khim.)*, 1986, **31**, 254.